



UNIVERSITY OF LEEDS

This is a repository copy of *Anomalous grain boundary conduction in BiScO₃-BaTiO₃ high temperature dielectrics*.

White Rose Research Online URL for this paper:
<https://eprints.whiterose.ac.uk/176898/>

Version: Accepted Version

Article:

Li, L, Roncal-Herrero, T, Harrington, J et al. (4 more authors) (2021) Anomalous grain boundary conduction in BiScO₃-BaTiO₃ high temperature dielectrics. *Acta Materialia*, 216. 117136. ISSN 1359-6454

<https://doi.org/10.1016/j.actamat.2021.117136>

© 2021, Elsevier. This manuscript version is made available under the CC-BY-NC-ND 4.0 license <http://creativecommons.org/licenses/by-nc-nd/4.0/>.

Reuse

This article is distributed under the terms of the Creative Commons Attribution-NonCommercial-NoDerivs (CC BY-NC-ND) licence. This licence only allows you to download this work and share it with others as long as you credit the authors, but you can't change the article in any way or use it commercially. More information and the full terms of the licence here: <https://creativecommons.org/licenses/>

Takedown

If you consider content in White Rose Research Online to be in breach of UK law, please notify us by emailing eprints@whiterose.ac.uk including the URL of the record and the reason for the withdrawal request.



eprints@whiterose.ac.uk
<https://eprints.whiterose.ac.uk/>

Anomalous grain boundary conduction in Bi₂O₃-rich BiScO₃-BaTiO₃ ceramics

Linhao Li¹, Teresa Roncal-Herrero², John Harrington², Steven J. Milne², Andy P. Brown², Julian S Dean¹ and Derek C Sinclair¹

1. Department of Materials Science and Engineering, University of Sheffield, Mappin St., Sheffield, S1 3JD, UK

2. School of Chemical and Process Engineering, University of Leeds, Leeds, LS2 9JT, UK

Abstract

A combination of X-ray Diffraction, analytical-Electron Microscopy, Differential Scanning Calorimetry, Impedance Spectroscopy (IS) and Electro-Motive-Force (EMF) measurements (for oxide-ion transport number measurements, t_{ion}) are used to report on the influence of a small amount of a continuous Bi₂O₃-rich phase along the grain boundaries in sample composition $x = 0.4$ (BS_{0.4}BT) for $x(\text{BiScO}_3)-(1-x)(\text{BaTiO}_3)$ (BS_{*x*}BT) high temperature (~ 200-500 °C) dielectric ceramics. Its presence produces a dramatic change in conductivity of ~ two orders of magnitude and a switch in t_{ion} over the range ~ 600 - 800 °C that is not observed for other ceramics with lower BiScO₃ content. Below ~ 700 °C the grain boundaries in BS_{0.4}BT act as electrically blocking layers and dominate the impedance of the ceramics. In contrast, > 800 °C the grain boundaries become highly conductive due to a polymorphic phase transition to, and melting of δ -Bi₂O₃ which results in the current percolating along the grain boundaries and therefore avoiding the grains. The value of t_{ion} increases from ~ 0.13 at ~ 600 °C to near unity at ~ 800 °C for BS_{0.4}BT consistent with oxide ion conduction at higher temperatures being due to the presence of liquid Bi₂O₃ at grain boundary regions. This behaviour was reproduced by adding a small excess of 3 wt% Bi₂O₃ into $x = 0.3$ (BS_{0.3}BT) samples to induce a Bi₂O₃-rich grain boundary phase, not otherwise present in this composition.

Introduction

In recent years there has been significant interest in the development of solid solutions between ferroelectric perovskites such as BaTiO₃ with BiMeO₃ perovskites, e.g. Me = Sc, Ti_{1/2}Mg_{1/2}, Ti_{1/2}Zn_{1/2}, to develop Pb-free temperature stable dielectrics for capacitor applications beyond 200 °C.[1–8] These include power electronics, engine communication and management systems in automobiles such as electric vehicles and devices operating under harsh environments (e.g. ~ 300 – 500 °C). The structure-composition-property relationships in these ABO₃ solid solutions have been intensively studied due to multiple site occupancy on both cation sublattices and segregation effects on either a micro- and/or nano-scopic scale.[9–17] Such phenomena can influence the short- and long-range order and coupling between the electric dipoles generated via A- and/or B-site displacements in the lattice(s) and therefore impact on the permittivity-temperature (ϵ -T) profiles. With increasing BiMeO₃ content (typically < 10 mol %) there is a cross over from classic ferroelectric behaviour in undoped BaTiO₃ with a very sharp peak in permittivity at the Curie Temperature to a core-shell type response (due to microscopic segregation) that generates a broadened ϵ -T profile with peaks associated with the core and shell regions in the microstructure.

At higher BiMeO₃ contents (typically 10 – 40 mol %), the core-shell type ϵ -T profiles (and microstructure) are replaced by highly diffuse and dispersive relaxor type ϵ -T profiles associated with polar nano regions (PNR's). This evolves into relatively temperature-stable ϵ -T profiles (for ~ 20-40 mol%) that exhibit weak relaxor behaviour at lower temperatures (typically < 100 °C) but a high ϵ -plateau (~ 500 – 1000) between ~ 150 and 500 °C. This makes these materials attractive for the aforementioned high temperature applications.

The initial objective of this study was to use Impedance Spectroscopy (IS) to probe the evolution of the grain electrical-microstructure, i.e. the switch from core/shell to NPR's in $x(\text{BiScO}_3)-(1-x)(\text{BaTiO}_3)$ (BS_xBT) with increasing BiScO₃-content, x (which will be addressed in a separate paper). During this study, however, we observed an anomalous high temperature conductivity behaviour for a composition BS_{0.4}BT close to the BiScO₃-end of the solid solution limit. This phenomenon is later proven here to be due to a grain boundary phase.

Grain boundaries often play a significant role in functional ceramics. In some cases, grain boundary functionality is desired and is central to performance whereas in others their contribution is deleterious and needs to be minimised. Examples of the former are the development of Schottky barriers at grain boundaries between semiconducting n-type grains in ZnO varistors [19] and positive temperature coefficient resistor (PTCR) BaTiO₃ thermistors [20,21]. Highly resistive grain boundaries are also beneficial in many dielectric ceramics. This is especially important for capacitor applications where dielectric layers are only a few micrometres in thickness. On the other hand, resistive grain boundaries are undesirable for some applications, such as solid electrolytes for electrochemical devices where there is a drive to minimise the total resistance of the electrolyte.

A commonly applied method to study grain and grain boundary impedances in electroceramics is Impedance Spectroscopy, IS. Since the pioneering IS work on Y-stabilised ZrO₂ ceramics by Baurele [22], simple equivalent circuit models based on a Brickwork Layer Model (BLM) approach often work well to extract bulk and grain boundary resistance and capacitance values for micron grain-sized ceramics where the grain boundaries are much more resistive than the grains [23–25]. Data analysis becomes more challenging when the volume fraction of grain boundary regions increases with decreasing grain size (as in nano grain-sized ceramics) and/or the grain boundary regions become more conductive than the grains [26–28]. The generic BLM assumes homogeneous grains (i.e. the bricks) in the form of a 3D array of regular cubes that are encased by homogeneous grain boundaries (i.e. the mortar), Fig 1 (a). A basic equivalent circuit to describe this electrical microstructure contains both series and parallel pathways, i.e. an outer grain boundary pathway that is connected in parallel with a series pathway based on upper and lower grain boundary regions with the grains, Fig 1 (b) (based on an applied voltage across the top and bottom of the sample). In the scenario where the grain boundaries are substantially more resistive than the grains, the equivalent circuit simplifies to only the series pathways with two parallel Resistor-Capacitor networks to represent the grains (or bulk) (R_b, C_b) and the grain boundaries ($R_{gb,s}, C_{gb,s}$) as there is negligible current via the grain boundaries in parallel pathways. This series model is often referred to as the S-BLM. As the grain boundaries become more conductive the parallel pathways become increasingly important and analysis of the IS data to extract bulk and grain boundary properties becomes challenging. This is often referred to as the series-parallel SP-BLM,

i.e. both the series-parallel path in Fig 1 (b). There have been several treatments of this type of scenario as documented elsewhere [26–29].

Although Bi-based oxides are commonly investigated for their dielectric properties, [1–8] some are also excellent oxide-ion conducting electrolytes [30–32]. The classic example is Bi_2O_3 which exhibits complex polymorphism and hysteresis in the polymorphic transitions [30]. The low temperature α -polymorph is a mixed p-type/oxide ion conductor (predominantly p-type) that transforms on heating to a face centred cubic δ -polymorph at 729 °C that is an excellent oxide-ion conducting electrolyte before melting at ~ 824 °C. There is a three order of magnitude increase in the conductivity associated with the α to δ transition from mS/cm to \sim S/cm and the conductivity of the δ -polymorph is comparable to that of the melt. On cooling, there is significant hysteresis in the δ to α transformation (typically ~ 80 - 90 °C) that is dependent on the cooling conditions. The transformation occurs via intermediate polymorphs β and/or γ in the range ~ 650 – 630 °C and these subsequently transform to α - Bi_2O_3 from ~ 650 – 490 °C. It is possible to stabilise δ - Bi_2O_3 at room temperature by rapid quenching from above the α to δ transition or to lower the transition temperature by chemical doping [31].

This script describes this anomalous behaviour observed in 0.4(BiScO_3)-0.6(BaTiO_3) that correlates with the presence of Bi_2O_3 -rich grain boundaries. These change from being highly resistive and inter-grain electrically blocking at lower temperatures (< 700 °C) to become percolative and highly (oxide-ion) conductive at high temperatures (> 800 °C). We propose this is linked to a combination of polymorphic phase transition(s) and melting of the Bi_2O_3 -rich grain boundary phase that occurs in the intermediate temperature range (~ 700 – 820 °C). Confirmation of this ‘switch’ from a grain boundary blocking series pathway (S-BLM) to a grain boundary conducting parallel pathway (SP-BLM) was obtained by engineering 0.3(BiScO_3)-0.7(BaTiO_3) ceramics with and without a Bi_2O_3 -rich grain boundary phase.

Experimental procedure

Ceramics were prepared by conventional solid-state synthesis. Bi_2O_3 (99.9%, Acros Organics), TiO_2 (99.9%, Sigma-Aldrich), BaCO_3 (99.5%, Sigma-Aldrich) and Sc_2O_3 powders (99.9%, Sigma-Aldrich) were used as raw materials. These were pre-dried for 16 h prior to weighing in appropriate amounts. The batched mixtures were ball milled in isopropanol with yttria-stabilized zirconia milling media for 6 h, dried, sieved and calcined at 800 °C for 2 h in air. The resultant powders were ball milled for 4 h followed by drying, sieving, a 2 h calcination at 850 °C and a further 6 h ball milling. Green pellets were formed by a uniaxial steel die and then isostatically pressed at 200 MPa. These were sintered at 1300 °C for 2 h in air. All pellets were covered in calcined powder of the same composition to minimise volatilisation during sintering.

X-ray powder diffraction (XRD) analysis was performed on sintered and crushed samples using a high-resolution STOE STADI-P diffractometer (Cu $K\alpha$ radiation). Microstructure and compositional analysis were determined by a combination of a Philips XL 30S FEG scanning electron microscope with a Noran energy dispersive X-ray analyser and subsequent TEM (described below). Ceramic samples for SEM were polished or polished and thermally etched at 90% of the sintering

temperature for 1 h before being coated with carbon. The melting and solidification process of a Bi_2O_3 phase was monitored with differential scanning calorimetry (DSC) using a Netzsch DSC 404 C Thermal analyser on sintered and crushed samples. The DSC experiments were performed under flowing air from 20 to 900 °C at a heating/cooling rates of 5 °C/min.

Samples were prepared for transmission electron microscopy (TEM) following two routes. First, by crushing a sintered pellet to a fine powder using an agate pestle and mortar. The powder was then dispersed in ethanol, sonicated for 2 minutes in an ultrasonic bath and drop-cast onto holey carbon film supported on 400 mesh copper finder grids (EM resolution Ltd). Second, by cutting a thin lamella using a Focused Ion Beam FEI Helios G4 CX Dual Beam microscope with in-situ-lift out onto dedicated support grids for TEM (Omniprobe Inc). Here, a final ion beam cleaning was done at 5 kV and 40 pA beam current to reduce any side-wall damage to the section. The nominal thickness of the lamella was ~ 50 nm, as measured by SEM imaging. All samples were analysed on a FEI Titan Themis³ G2 transmission electron microscope operated at 300 kV with a monochromator, a Super-X 4-detector silicon drift energy dispersive X-ray (EDX) system. High angle annular dark field (HAADF) images were collected over the scattering semi-angle range of 35-150 mrad. STEM was run with a 1.4 Å probe diameter of 10 mrad convergence semi angle; probe currents were varied by the monochromator (not excited) and ranged from 40 – 200 pA depending on the imaging and mapping mode. EDX spectra were processed in Velox 2.1 and elemental quantification undertaken using the standard-less method within the software, involving estimation of thickness, density and fitting of Brown-Powell cross-sections with a ± 2 eV uncertainty.

Impedance spectroscopy was performed on sintered ceramics coated with Au-paste electrodes using a Solartron Modulab and a Hewlett Packard 4284A Precision LCR meter. The data were corrected for sample geometry (thickness/area). Oxygen ion transport number was taken via electromotive force (EMF) method on a ProboStat system at 600–800 °C. A gas concentration cell was prepared using N_2 and air to generate an oxygen partial pressure ($p\text{O}_2$) gradient. A YSZ tube was used as a $p\text{O}_2$ monitor as described previously [33].

In the following text sample compositions $x(\text{BiScO}_3)-(1-x)(\text{BaTiO}_3)$ are labelled as BS_xBT , where x represents the mole fraction of BiScO_3 , $x = 0.2, 0.3$ and 0.4 , and $0.3(\text{BiScO}_3)-0.7(\text{BaTiO}_3) + 3\text{wt}\%$ Bi_2O_3 is labelled as $\text{BS}_{0.3}\text{BT-Bi}$.

Results

The XRD patterns of BS_xBT ceramics for $x = 0.2-0.4$ are displayed in Fig 2 (a). Diffraction patterns could be fully indexed using a cubic cell (space group Pm-3m) for all samples except for $\text{BS}_{0.4}\text{BT}$ where an additional low intensity peak at $28.3^\circ 2\theta$ indicates the presence of $\beta\text{-Bi}_2\text{O}_3$ (ICSD: 62979) as a secondary phase. A small increase in lattice parameter was observed with increasing BiScO_3 (BS) content, Fig 2 (b). The density is relatively low for $\text{BS}_{0.2}\text{BT}$ (84%) ceramics due to the sintering temperature used but ceramic density significantly improved for $\text{BS}_{0.3}\text{BT}$ and $\text{BS}_{0.4}\text{BT}$ (reaching $>94\%$), Fig 2 (b).

SEM images of thermally etched BS_xBT ceramics are shown in Fig 3 (a-c). The grain size is

between 2-5 μm in $\text{BS}_{0.2}\text{BT}$ and 5-10 μm in $\text{BS}_{0.3}\text{BT}$ and $\text{BS}_{0.4}\text{BT}$. The presence of a Bi_2O_3 phase in $\text{BS}_{0.4}\text{BT}$ was further confirmed by a combination of SEM/EDX and TEM with an additional Sc_2O_3 phase also being detected by SEM, Fig 3 (f) and (g). The Bi_2O_3 and Sc_2O_3 phases are mainly accumulated at grain boundary triple pockets as these are identified to be Bi, Sc and O rich by EDX, Fig 3 (f). TEM images show these islands are connected via very thin (<2 nm) layers rich in Bi and O along grain boundaries, Fig 3 (g). Samples of $\text{BS}_{0.3}\text{BT}$ appeared phase pure by SEM and TEM with no evidence of Bi and O enrichment along the grain boundaries, Fig 3 (d) and (e), which agrees with the XRD results in Fig 2 (a).

The DSC data on $\text{BS}_{0.4}\text{BT}$ showed clear evidence of an endothermic process occurring on heating with an onset temperature of ~ 818 $^\circ\text{C}$ and an exothermic process with an onset temperature of ~ 799 $^\circ\text{C}$ on cooling, Fig. 4. There were no DSC thermal events observed on heating/cooling for $\text{BS}_{0.2}\text{BT}$ over the same temperature range and although no clear DSC peaks were observed for $\text{BS}_{0.3}\text{BT}$ there were significant changes in the baseline slope at ~ 818 $^\circ\text{C}$ and ~ 799 $^\circ\text{C}$ on the heating and cooling cycles, respectively, Fig 4.

The temperature dependent relative permittivity (ϵ_r) and dielectric loss ($\tan \delta$) from room temperature to ~ 850 $^\circ\text{C}$ are shown in Fig 5. A broad, relatively temperature-insensitive permittivity response is observed in all three BS-BT ceramics. The maximum permittivity (ϵ_{max}) increases from ~ 850 for $\text{BS}_{0.2}\text{BT}$ to ~ 1100 for $\text{BS}_{0.4}\text{BT}$. The value of $\tan \delta$ of all three samples is low (< 0.02) within the temperature range 200 – 400 $^\circ\text{C}$. At higher temperatures (> 400 $^\circ\text{C}$), both the ϵ_r and $\tan \delta$ values of $\text{BS}_{0.4}\text{BT}$ show hysteresis behaviour on heating and cooling, which was not observed for $\text{BS}_{0.2}\text{BT}$ and $\text{BS}_{0.3}\text{BT}$.

The EMF method was used to measure the oxygen-ion transport number (t_{ion}) of the ceramics in the range of ~ 600 to 900 $^\circ\text{C}$. The value of t_{ion} was negligible for $\text{BS}_{0.2}\text{BT}$ (~ 0.02) indicating the ceramics were predominantly electronically conducting over this temperature range whereas $\text{BS}_{0.3}\text{BT}$ ceramics gave $t_{\text{ion}} \sim 0.17$ indicating mixed ionic-electronic conduction. In contrast, t_{ion} of $\text{BS}_{0.4}\text{BT}$ was very temperature dependent. It was low (< 0.25) at temperatures < 650 $^\circ\text{C}$ but increased rapidly above 700 $^\circ\text{C}$ and approached unity at temperatures ≥ 800 $^\circ\text{C}$, Fig 6 (c). This indicates mixed ionic-electronic conduction at ~ 650 $^\circ\text{C}$ and is replaced by oxide-ion conduction in these ceramics at ~ 800 $^\circ\text{C}$. It is noteworthy that the rapid change in t_{ion} with temperature occurs over the same temperature range as the hysteresis in the ϵ_r data, Fig 5. To investigate the electrical properties in more detail, IS was performed on all of these ceramics. The aim was not to fully fit the data using equivalent circuit analysis but rather to assess the total conductivity (σ_T) of the BS_xBT ceramics based on inspection of Z^* plots and to identify the presence and/or absence of electronic and/or ionic conduction. This involved: (i) identifying (where possible) bulk and grain boundary responses by the presence of high and intermediate frequency Z^* arcs with appropriate associated capacitance values [34]; (ii) identifying ionic or mixed ionic-electronic conduction via the presence and/or absence of a finite or infinite Warburg response respectively at low frequencies in the Z^* plots [35]; (iii) taking σ_T as the reciprocal of the low frequency intercept on the real axis of Z^* plots between the ceramic and electrode responses (preceding points (i) and (ii), respectively).

The Z^* response for $\text{BS}_{0.2}\text{BT}$ at 600 $^\circ\text{C}$ consisted of a single, large arc with an associated capacitance of ~ 37 pF/cm and little evidence of any significant low frequency electrode response

associated with mixed conduction, Fig 6 (a) and Fig S1 (a). The Z^* response at 900 °C consists of a partial arc, Fig 6 (b); however, closer inspection of the low frequency data indicated the presence of a very small electrode effect that was difficult to resolve and could not be investigated in detail, Fig 6 (b) and Fig S1(b). The impedance data for $BS_{0.2}BT$ are consistent with σ_T being a bulk-type response. The absence of any significant electrode effects in Z^* in combination with the negligible t_{ion} values indicate the bulk conduction to be electronic. An Arrhenius plot of σ_T for $BS_{0.2}BT$ gives a linear response with an activation energy (E_a) for the bulk conduction of ~ 1.22 eV.

The Z^* response for $BS_{0.3}BT$ at 600 °C was significantly different to that observed for $BS_{0.2}BT$. At 600 °C the data show clear evidence of two poorly resolved large arcs in Z^* , Fig 6 (a), with evidence on closer inspection of a third, much smaller but significantly broadened arc response at lower frequencies, Fig S1 (c). The high frequency arc in Z^* has an associated capacitance of ~ 40 pF/cm which is similar in magnitude to that observed for $BS_{0.2}BT$ at the same temperature, Fig 6 (a) and is therefore attributed to a bulk response. The additional large arc at lower frequencies for $BS_{0.3}BT$ has an associated capacitance of ~ 150 pF/cm and is attributed to a grain boundary response, Fig 6 (a). As a consequence of the grain boundary impedance, σ_T is about a factor of two lower for $BS_{0.3}BT$ when compared to $BS_{0.2}BT$ at 600 °C. The third arc at lower frequency has an associated capacitance of ~ 25 nF/cm and is attributed to an electrode effect associated with diffusion of oxide ions at the ceramic/electrode interface, Fig S1(c). The Z^* response at 900 °C for $BS_{0.3}BT$ also shows a partial arc, Fig 6 (b) that is associated with the response from the ceramic and clear evidence of the ceramic/electrode interface Z^* response at lower frequency. The impedance data for $BS_{0.3}BT$ ceramics are therefore consistent with σ_T being a combined bulk and grain boundary type response. The presence of the electrode effects in Z^* in combination with $t_{ion} \sim 0.17$ confirms the conduction behaviour in the ceramics to be mixed ionic-electronic conduction. An Arrhenius plot of σ_T for $BS_{0.3}BT$ gives a very similar trend and E_a to that obtained for $BS_{0.2}BT$, Fig 6 (c) indicating that bulk conduction dominates σ_T over the measured range from 600 -900 °C.

For $BS_{0.4}BT$ there was a large asymmetric arc that was at least one order of magnitude greater at 600 °C compared with $BS_{0.2}BT$ or $BS_{0.3}BT$. In this case, it was not possible to resolve or identify bulk or grain boundary components from Z^* plots and this response was attributed to the overall ceramic such that σ_T at 600 °C was significantly lower for $BS_{0.4}BT$ compared to $BS_{0.2}BT$ and $BS_{0.3}BT$. Closer inspection of the low frequency data in the Z^* plot did not indicate the presence of a significant response associated with a ceramic/electrode interface effect, Fig S1 (d); however, this could have been masked by the large impedance response associated with the ceramic at 600 °C. In contrast, the Z^* response for $BS_{0.4}BT$ at 900 °C had the lowest impedance of all the BS-BT ceramics, Fig 6 (b), with the response being dominated by a low frequency spike associated with Warburg diffusion (~ 450 $\mu F/cm$) indicating the presence of ionic conduction. An Arrhenius plot of σ_T for $BS_{0.4}BT$ showed anomalous behaviour that could be subdivided into three regions with E_a values of ~ 1.84 eV (<750 °C), 5.43 eV ($\sim 750-875$ °C) and 0.58 eV (>875 °C). It is noteworthy that all E_a values are very different to those obtained for $BS_{0.2}BT$ and $BS_{0.3}BT$ (~ 1.22 eV). Combining the impedance data with the variation in t_{ion} from ~ 0.25 at 600 °C to near unity $> \sim 775$ °C, shows $BS_{0.4}BT$ ceramics exhibit mixed ionic-electronic conduction at 600 °C but are ionically conducting above ~ 800 °C. Given the clear evidence for a Bi_2O_3 -rich grain boundary phase in $BS_{0.4}BT$ from the XRD pattern and Electron Microscopy shown in Figs 2 and 3, and its absence in $BS_{0.2}BT$ and $BS_{0.3}BT$, we prepared a new batch of $BS_{0.3}BT$ with an additional 3wt.% Bi_2O_3 in the starting composition, i.e.

BS_{0.3}BT-Bi. The aim being to induce a Bi₂O₃-rich grain boundary phase and to use this to assess the influence of the grain boundary modification on the electrical properties.

The XRD data for BS_{0.3}BT and BS_{0.3}BT-Bi show no evidence of any additional reflections associated with the excess Bi sample, BS_{0.3}BT-Bi, Fig 7 (a). This result for BS_{0.3}BT-Bi is in contrast to BS_{0.4}BT where the presence of β -Bi₂O₃ was visible by XRD, Fig 2(a). There is a small decrease in the lattice parameter and a modest increase in the density of the ceramics for BS_{0.3}BT-Bi compared to BS_{0.3}BT, inset Fig 7 (a). The grain sizes of BS_{0.3}BT-Bi were in the range of 7-15 μ m which are slightly larger compared to BS_{0.3}BT, Fig 7 (b). The SEM back-scattering images revealed bright regions of contrast associated with a secondary phase in BS_{0.3}BT-Bi and EDX confirmed this to be Bi and O rich i.e. Bi₂O₃, Fig 7 (c). Furthermore, TEM revealed clear Bi-enrichment in triple pockets areas and along the grain boundaries in BS_{0.3}BT-Bi, Fig 7 (c). These results confirm the presence of a Bi-rich grain boundary phase in BS_{0.3}BT-Bi ceramics that is similar to that observed for BS_{0.4}BT, Fig 3 (f) and (g). The inability of XRD to detect Bi₂O₃ in BS_{0.3}BT-Bi compared to BS_{0.4}BT is therefore attributed to either a lower amount of this phase or it being amorphous in BS_{0.3}BT ceramics. DSC data revealed exothermic and endothermic processes for BS_{0.3}BT-Bi on heating and cooling, respectively at the same temperatures as those observed for BS_{0.4}BT, Fig 4. The DSC peaks are less pronounced for BS_{0.3}BT-Bi compared to BS_{0.4}BT which is consistent with a lower level and/or amorphous Bi₂O₃ being present in BS_{0.3}BT and is also consistent with the XRD data in Fig 2 (a) and Fig 7 (a). The absence of any evidence of second phase Bi₂O₃ in BS_{0.3}BT by XRD but the presence of small anomalies in the corresponding DSC traces at \sim 818 and \sim 799 $^{\circ}$ C on heating and cooling, respectively suggest there are low levels of Bi₂O₃ (amorphous or crystalline) in BS_{0.3}BT, Fig 4.

The dielectric properties of BS_{0.3}BT and BS_{0.3}BT-Bi are broadly in agreement over the temperature range from RT to \sim 600 $^{\circ}$ C, Fig 8; however, there are significant deviations above 600 $^{\circ}$ C for BS_{0.3}BT-Bi. The ϵ_r data show an anomalous dip commencing at \sim 700 $^{\circ}$ C and both ϵ_r and $\tan \delta$ display hysteresis on heating and cooling in this high temperature range, Fig 8. The Z^* plots for BS_{0.3}BT-Bi at 600 $^{\circ}$ C and 900 $^{\circ}$ C are shown in Figs. 8 (a) and (b), respectively. In contrast to BS_{0.3}BT, where bulk and grain boundary responses can be resolved, only a large and asymmetric arc is present in BS_{0.3}BT-Bi at 600 $^{\circ}$ C with σ_T being at least a factor of two lower for BS_{0.3}BT-Bi, Fig 9 (a). In contrast, Z^* plots for 900 $^{\circ}$ C show BS_{0.3}BT-Bi to be less resistive than BS_{0.3}BT with the presence of a low angle spike at low frequencies, inset Fig 9 (b). The Arrhenius plot of σ_T for BS_{0.3}BT-Bi in Fig 9 (c), reveals similar anomalous behaviour to that observed for BS_{0.4}BT and can be subdivided into three regions based on changes in E_a . Although the values of E_a are different, the trend is the same in BS_{0.3}BT-Bi and BS_{0.4}BT, i.e. in the former E_a changes from \sim 1.88 eV ($<$ 750 $^{\circ}$ C) to \sim 3.55 eV (750-850 $^{\circ}$ C) and eventually \sim 0.31 eV ($>$ 850 $^{\circ}$ C) on heating and in the latter E_a changes from \sim 1.84 eV ($<$ 750 $^{\circ}$ C) to 5.43 eV (\sim 750-875 $^{\circ}$ C) and finishes at 0.58 eV ($>$ 875 $^{\circ}$ C). The t_{ion} of BS_{0.3}BT-Bi also increases rapidly with increasing temperature and reaches $>$ 0.96 at temperatures $>$ 800 $^{\circ}$ C, Fig 9 (c). This confirms a switch from mixed ionic-electronic conduction at \sim 600 $^{\circ}$ C to predominantly oxide-ion conduction at \sim 800 $^{\circ}$ C, Fig 9 (c). In summary, the anomalous high temperature conduction properties observed for BS_{0.4}BT and the exothermic and endothermic events observed in DSC data were successfully reproduced by adding a small excess of Bi₂O₃ into BS_{0.3}BT. This indicates the high σ_T and t_{ion} at high temperature, the change of E_a with temperature and the hysteresis behaviour of ϵ_r and $\tan \delta$ in BS_{0.4}BT are associated with the presence of the Bi₂O₃ secondary phase located in the triple points and along grain boundaries in the ceramics.

Discussion

As the BiScO_3 content increases within the x -series of ceramics $x(\text{BiScO}_3)-(1-x)(\text{BaTiO}_3)$ (without the addition of any excess Bi_2O_3) the influence of the grain boundary regions on σ_T and t_{ion} become increasingly important. Based on the XRD and Electron Microscopy data, Figs 2 and 3, the BS_xBT solid solution limit is reached at $x \sim 0.3$ ($\text{BS}_{0.3}\text{BT}$). This is in reasonable agreement with that reported previously [3] and our data show that beyond the solid solution limit, Bi_2O_3 (and to a lesser extent Sc_2O_3) reside in triple points and grain boundary regions. For $\text{BS}_{0.4}\text{BT}$ there is sufficient excess Bi_2O_3 to form a continuous (or a near continuous) network along the grain boundaries and at the triple points, Fig 3 (f) and (g). Because σ_T and E_a of $\text{BS}_{0.2}\text{BT}$ and $\text{BS}_{0.3}\text{BT}$ are relatively similar (more so for their bulk conductivity) and since the solid solution limit is at $x \sim 0.3$, it is reasonable to expect that the bulk conductivity of $\text{BS}_{0.4}\text{BT}$ should be similar to $\text{BS}_{0.2}\text{BT}$ and $\text{BS}_{0.3}\text{BT}$. Therefore, we propose that these Bi_2O_3 -rich grain boundary regions are resistive at lower temperatures (e.g. < 600 °C) and dominate the Z^* response, Fig 6 (a) inset, and σ_T of the ceramics, Fig 6 (c). This would suggest an equivalent circuit (to a first approximation) based on a series pathway in Fig 1 (b) is the most appropriate model to start any detailed studies on trying to deconvolute σ_T into bulk and grain boundary components. The dramatic increase in t_{ion} from ~ 0.25 to near unity in the range ~ 675 °C to 775 °C suggests transformation to the oxide-ion conducting δ - Bi_2O_3 polymorph is occurring. This transition was not observed by DSC; however, melting of the Bi_2O_3 -rich phase was observed and occurs at ~ 820 °C, Fig 4. Therefore, we attribute the switch over in σ_T in the Arrhenius plot for $\text{BS}_{0.4}\text{BT}$ ceramics in the range $\sim 750 - 875$ °C with $E_a \sim 5.5$ eV to be associated with the polymorphic and state of matter changes in the Bi_2O_3 -rich grain boundary regions.

Above 850 °C the most appropriate equivalent circuit to analyse IS data would be based (to a first approximation) on a single parallel $R_{\text{gb,p}}C_b$ element connected in series with a Warburg element. This would reflect the physical situation of the permittivity associated with the grains (C_b) combined with the short-circuiting, parallel pathway ($R_{\text{gb,p}}$, see Fig 1 (b)) associated with a highly oxide ion conducting liquid Bi_2O_3 network along the grain boundaries. Proposing an equivalent circuit or plausible equivalent circuits for the intermediate temperature region is beyond the scope of the present work but would require the use of both parallel and series conduction pathways, Fig 1 (b).

In contrast, $\text{BS}_{0.2}\text{BT}$ ceramics show only a bulk response in Z^* plots, Fig 6 (a) with no evidence of a grain boundary phase by Electron Microscopy or any phase transitions in DSC, Fig 4. Linear Arrhenius-type behaviour is observed for σ_T , Fig 6 (c) and when combined with the negligible t_{ion} across the measured temperature range indicates $\text{BS}_{0.2}\text{BT}$ is electronically insulating with $E_a \sim 1.22$ eV. This behaviour is consistent with the expected dielectric behaviour for stoichiometric BS_xBT ceramics.

The case of $\text{BS}_{0.3}\text{BT}$ is interesting. A grain boundary response is apparent in Z^* at 600 °C but it doesn't dominate σ_T or cause a switch in σ_T at higher temperatures, Fig 6. However, the transport number is significantly higher compared to $\text{BS}_{0.2}\text{BT}$ and there is a change in baseline slope but no clear peaks in the DSC at high temperatures, Fig 4. This suggests some Bi_2O_3 -rich grain boundaries

are present but that they never form an interconnected liquid network at higher temperatures to cause a sufficient parallel conducting network that allows by-passing of the grain (electronic) response. This would explain why switching of σ_T is not observed. Additional support for this hypothesis is that σ_T and the associated E_a for $BS_{0.3}BT$ is very similar to $BS_{0.2}BT$, Fig 6 (c). If a grain response was responsible for the t_{ion} , then a change in σ_T and E_a for these two compositions would be expected but is not observed.

DSC, Electron Microscopy, IS and t_{ion} data for $BS_{0.3}BT$ -Bi (Bi-excess) ceramics clearly support the proposal that the switch in conduction type and level of conductivity is associated with the presence of a Bi_2O_3 -rich grain boundary phase that melts at ~ 820 °C, figures 4, 7 and 9, respectively. The hysteresis between ~ 600 and 800 °C in the 1 MHz ϵ_r and $\tan \delta$ data on heating and cooling in $BS_{0.4}BT$ and $BS_{0.3}BT$ -Bi also support this hypothesis, Figs 5 and 8, respectively. It is important to stress this unusual electrical behaviour is a high temperature phenomenon and doesn't influence the ϵ_r and $\tan \delta$ properties of BS_xBT ceramics at temperatures of < 400 °C where they are being considered for capacitor applications. In fact, σ_T of $BS_{0.4}BT$ and $BS_{0.3}BT$ -Bi below 400 °C is lower than $BS_{0.2}BT$ and $BS_{0.3}BT$, Fig 6 (c) and 9, and is therefore beneficial for their low field insulation resistance and possibly their breakdown strength depending on how the electric field is distributed in these ceramics.

Bismuth oxide grain boundary wetting that gives rise to enhanced ionic diffusion and conductivity has been reported previously. For example, Bi_2CuO_4 - Bi_2O_3 composite ceramics show similar anomalous rises in high temperature transport properties (occurring at ~ 730 and 770 °C) that are attributed to the α - to δ -polymorphic transition and melting of Bi_2O_3 at the grain boundaries, respectively, and result in parallel conduction pathways throughout the ceramics [36]. It is noteworthy that anomalous jumps in electrical conductivity at ~ 770 °C have recently been reported for Sr-doped $BiFeO_3$ ceramics [37]. In this case, the behaviour was attributed to a bulk-related phenomenon as opposed to a grain boundary effect. No information was provided as to whether or not there was Bi_2O_3 segregation at the grain boundaries in those ceramics and this may merit further investigation.

The phenomenon we describe here may be common in Bi-based oxides processed by solid state reactions because of the volatility and low melting point of Bi_2O_3 as a starting reagent. To suppress and/or compensate for this volatilisation, it is common practice to either add a small excess of Bi_2O_3 to the nominal starting stoichiometry [3] and/or to cover pellets with sacrificial powder prior to sintering of ceramics [32]. Bi_2O_3 however can also act as a sintering aid and therefore assist with densification of ceramics [34].

In conclusion, we highlight a potential grain boundary conduction issue surrounding functional ceramics based on Bi-based oxides such as BS_xBT or where Bi_2O_3 is added as a sintering aid. If excess Bi_2O_3 is present as a secondary phase and is distributed along grain boundaries then high temperature polymorphic phase transitions and melting (at ~ 820 °C) can induce high levels of oxide-ion conductivity that can significantly influence the high temperature electrical properties.

Acknowledgments

We thank the EPSRC for funding Analysis of Polar Nanostructures in High Temperature Relaxor Dielectrics: A Framework for Materials Discovery (EP/P015514/1 and EP/P015565/1).

References

- [1] C.C. Huang, D.P. Cann, X. Tan, N. Vittayakorn, Phase transitions and ferroelectric properties in $\text{BiScO}_3\text{-Bi}(\text{Zn}_{1/2}\text{Ti}_{1/2})\text{O}_3\text{-BaTiO}_3$ solid solutions, *J. Appl. Phys.* 102 (2007) 044103. <https://doi.org/10.1063/1.2769787>.
- [2] C.C. Huang, D.P. Cann, Phase transitions and dielectric properties in $\text{Bi}(\text{Zn}_{1/2}\text{Ti}_{1/2})\text{O}_3\text{-BaTiO}_3$ perovskite solid solutions, *J. Appl. Phys.* 104 (2008) 024117. <https://doi.org/10.1063/1.2960469>.
- [3] H. Ogihara, C.A. Randall, S. Trolier-McKinstry, Weakly coupled relaxor behavior of $\text{BaTiO}_3\text{-BiScO}_3$ ceramics, *J. Am. Ceram. Soc.* 92 (2009) 110–118. <https://doi.org/10.1111/j.1551-2916.2008.02798.x>.
- [4] Q. Zhang, Z. Li, F. Li, Z. Xu, Structural and Dielectric Properties of $\text{Bi}(\text{Mg}_{1/2}\text{Ti}_{1/2})\text{O}_3\text{-BaTiO}_3$ Lead-Free Ceramics, *J. Am. Ceram. Soc.* 94 (2011) 4335–4339. <https://doi.org/10.1111/j.1551-2916.2011.04695.x>.
- [5] A. Zeb, S.J. Milne, Dielectric and Piezoelectric Properties of $(1-x)\text{K}_{0.5}\text{Bi}_{0.5}\text{TiO}_3-x\text{Ba}(\text{Ti}_{0.8}\text{Zr}_{0.2})\text{O}_3$ Ceramics, *J. Am. Ceram. Soc.* 96 (2013) 3089–3093. <https://doi.org/10.1111/jace.12425>.
- [6] A. Zeb, S.J. Milne, Stability of High-Temperature Dielectric Properties for $(1-x)\text{Ba}_{0.8}\text{Ca}_{0.2}\text{TiO}_3-x\text{Bi}(\text{Mg}_{0.5}\text{Ti}_{0.5})\text{O}_3$ Ceramics, *J. Am. Ceram. Soc.* 96 (2013) 2887–2892. <https://doi.org/10.1111/jace.12412>.
- [7] A. Zeb, Y. Bai, T. Button, S.J. Milne, Temperature-Stable Relative Permittivity from -70°C to 500°C in $(\text{Ba}_{0.8}\text{Ca}_{0.2})\text{TiO}_3\text{-Bi}(\text{Mg}_{0.5}\text{Ti}_{0.5})\text{O}_3\text{-NaNbO}_3$ Ceramics, *J. Am. Ceram. Soc.* 97 (2014) 2479–2483. <https://doi.org/10.1111/jace.12949>.
- [8] A. Zeb, S.J. Milne, High temperature dielectric ceramics: a review of temperature-stable high-permittivity perovskites, *J. Mater. Sci. Mater. Electron.* 26 (2015) 9243–9255. <https://doi.org/10.1007/s10854-015-3707-7>.
- [9] D.S. Tinberg, S. Trolier-Mckinstry, Structural and electrical characterization of $x\text{BiScO}_3\text{-(1-x)}\text{BaTiO}_3$ thin films, *J. Appl. Phys.* 101 (2007) 024112. <https://doi.org/10.1063/1.2430627>.
- [10] S. Trolier-Mckinstry, M.D. Biegalski, J. Wang, A.A. Belik, E. Takayama-Muromachi, I. Levin, Growth, crystal structure, and properties of epitaxial BiScO_3 thin films, *J. Appl. Phys.* 104 (2008) 044102. <https://doi.org/10.1063/1.2964087>.
- [11] K. Datta, P.A. Thomas, Structural investigation of a novel perovskite-based lead-free ceramics: $\text{XBiScO}_3\text{-(1-x)}\text{BaTiO}_3$, *J. Appl. Phys.* 107 (2010) 043516. <https://doi.org/10.1063/1.3309064>.
- [12] S.S.N. Bharadwaja, J.R. Kim, H. Ogihara, L.E. Cross, S. Trolier-McKinstry, C.A. Randall, Critical

- slowing down mechanism and reentrant dipole glass phenomena in $(1-x)\text{BaTiO}_3x\text{BiScO}_3$ ($0.1 \leq x \leq 0.4$): The high energy density dielectrics, *Phys. Rev. B.* 83 (2011) 024106. <https://doi.org/10.1103/PhysRevB.83.024106>.
- [13] H. Takenaka, I. Grinberg, S. Liu, A.M. Rappe, Slush-like polar structures in single-crystal relaxors, *Nature.* 546 (2017) 391–395. <https://doi.org/10.1038/nature22068>.
- [14] V. Krayzman, I. Levin, J.C. Woicik, F. Bridges, Correlated rattling-ion origins of dielectric properties in reentrant dipole glasses BaTiO_3 - BiScO_3 , *Appl. Phys. Lett.* 107 (2015) 192903. <https://doi.org/10.1063/1.4935417>.
- [15] I. Levin, V. Krayzman, J.C. Woicik, F. Bridges, G.E. Sterbinsky, T.M. Usher, J.L. Jones, D. Torrejon, Local structure in BaTiO_3 - BiScO_3 dipole glasses, *Phys. Rev. B.* 93 (2016) 104106. <https://doi.org/10.1103/PhysRevB.93.104106>.
- [16] T.M. Usher, T. Iamsasri, J.S. Forrester, N. Raengthon, N. Triamnak, D.P. Cann, J.L. Jones, Local and average structures of BaTiO_3 - $\text{Bi}(\text{Zn}_{1/2}\text{Ti}_{1/2})\text{O}_3$, *J. Appl. Phys.* 120 (2016) 184102. <https://doi.org/10.1063/1.4967222>.
- [17] T. Roncal-Herrero, J. Harrington, A. Zeb, S.J. Milne, A.P. Brown, Nanoscale compositional segregation and suppression of polar coupling in a relaxor ferroelectric, *Acta Mater.* 158 (2018) 422–429. <https://doi.org/10.1016/j.actamat.2018.07.053>.
- [18] K. Hong, T.H. Lee, J.M. Suh, S.H. Yoon, H.W. Jang, Perspectives and challenges in multilayer ceramic capacitors for next generation electronics, *J. Mater. Chem. C.* 7 (2019) 9782–9802. <https://doi.org/10.1039/c9tc02921d>.
- [19] L.M. Levinson, H.R. Philipp, Zinc oxide varistors — a review, *Am. Ceram. Soc. Bull.* 65 (1986) 639–646.
- [20] W. Heywang, Bariumtitanat als sperrschichtbleiter, *Solid State Electron.* 3 (1961) 51–58. [https://doi.org/10.1016/0038-1101\(61\)90080-6](https://doi.org/10.1016/0038-1101(61)90080-6).
- [21] G.H. Jonker, Some aspects of semiconducting barium titanate, *Solid State Electron.* 7 (1964) 895–903. [https://doi.org/10.1016/0038-1101\(64\)90068-1](https://doi.org/10.1016/0038-1101(64)90068-1).
- [22] J.E. Bauerle, Study of solid electrolyte polarization by a complex admittance method, *J. Phys. Chem. Solids.* 30 (1969) 2657–2670. [https://doi.org/10.1016/0022-3697\(69\)90039-0](https://doi.org/10.1016/0022-3697(69)90039-0).
- [23] N.M. Beekmans, L. Heyne, Correlation between impedance, microstructure and composition of calcia-stabilized zirconia, *Electrochim. Acta.* 21 (1976) 303–310. [https://doi.org/10.1016/0013-4686\(76\)80024-2](https://doi.org/10.1016/0013-4686(76)80024-2).
- [24] T. van Dijk, A.J. Burggraaf, Grain boundary effects on ionic conductivity in ceramic $\text{Gd}_x\text{Zr}_{1-x}\text{O}_{2-(x/2)}$ solid solutions, *Phys. Status Solidi.* 63 (1981) 229–240. <https://doi.org/10.1002/pssa.2210630131>.

- [25] M. VERKERK, B. MIDDELHUIS, A. BURGGRAAF, Effect of grain boundaries on the conductivity of high-purity $\text{ZrO}_2\text{-Y}_2\text{O}_3$ ceramics, *Solid State Ion.* 6 (1982) 159–170. [https://doi.org/10.1016/0167-2738\(82\)90083-2](https://doi.org/10.1016/0167-2738(82)90083-2).
- [26] H. Näfe, Ionic conductivity of ThO_2 - and ZrO_2 -based electrolytes between 300 and 2000 K, *Solid State Ion.* 13 (1984) 255–263. [https://doi.org/10.1016/0167-2738\(84\)90040-7](https://doi.org/10.1016/0167-2738(84)90040-7).
- [27] J. Fleig, J. Maier, A Finite Element Study on the Grain Boundary Impedance of Different Microstructures, *J. Electrochem. Soc.* 145 (1998) 2081–2089. <https://doi.org/10.1149/1.1838600>.
- [28] N.J. Kidner, N.H. Perry, T.O. Mason, E.J. Garboczi, The Brick Layer Model Revisited: Introducing the Nano-Grain Composite Model, *J. Am. Ceram. Soc.* 91 (2008) 1733–1746. <https://doi.org/10.1111/j.1551-2916.2008.02445.x>.
- [29] J.P. Heath, J.H. Harding, D.C. Sinclair, J.S. Dean, The Analysis of Impedance Spectra for Core–Shell Microstructures: Why a Multiformalism Approach is Essential, *Adv. Funct. Mater.* 29 (2019) 1904036. <https://doi.org/10.1002/adfm.201904036>.
- [30] H.A. Harwig, A.G. Gerards, Electrical properties of the α , β , γ , and δ phases of bismuth sesquioxide, *J. Solid State Chem.* 26 (1978) 265–274. [https://doi.org/10.1016/0022-4596\(78\)90161-5](https://doi.org/10.1016/0022-4596(78)90161-5).
- [31] N.M. Sammes, G.A. Tompsett, H. Näfe, F. Aldinger, Bismuth based oxide electrolytes— structure and ionic conductivity, *J. Eur. Ceram. Soc.* 19 (1999) 1801–1826. [https://doi.org/10.1016/S0955-2219\(99\)00009-6](https://doi.org/10.1016/S0955-2219(99)00009-6).
- [32] F. Yang, M. Li, L. Li, P. Wu, E. Pradal-Velázquez, D.C. Sinclair, Review: Defect chemistry and electrical properties of sodium bismuth titanate perovskite, *J. Mater. Chem. A.* (2018). <https://doi.org/10.1039/C7TA09245H>.
- [33] M. Li, M.J. Pietrowski, R.A. De Souza, H. Zhang, I.M. Reaney, S.N. Cook, J.A. Kilner, D.C. Sinclair, A family of oxide ion conductors based on the ferroelectric perovskite $\text{Na}_{0.5}\text{Bi}_{0.5}\text{TiO}_3$, *Nat. Mater.* 13 (2014) 31–35. <https://doi.org/10.1038/nmat3782>.
- [34] J.T.S. Irvine, D.C. Sinclair, A.R. West, Electroceramics: characterization by impedance spectroscopy, *Adv. Mater.* 2 (1990) 132–138. <https://doi.org/10.1002/adma.19900020304>.
- [35] J. Jamnik, J. Maier, Treatment of the Impedance of Mixed Conductors Equivalent Circuit Model and Explicit Approximate Solutions, *J. Electrochem. Soc.* 146 (1999) 4183–4188. <https://doi.org/10.1149/1.1392611>.
- [36] V.V. Belousov, Surface ionics: A brief review, *J. Eur. Ceram. Soc.* 27 (2007) 3459–3467. <https://doi.org/10.1016/j.jeurceramsoc.2007.01.014>.
- [37] Y. Tomura, I. Oikawa, H. Takamura, Oxygen vacancy order-disorder transition at high temperature in Bi-Sr-Fe-based perovskite-type oxides, *Phys. Rev. Mater.* 3 (2019) 125802.

Figures

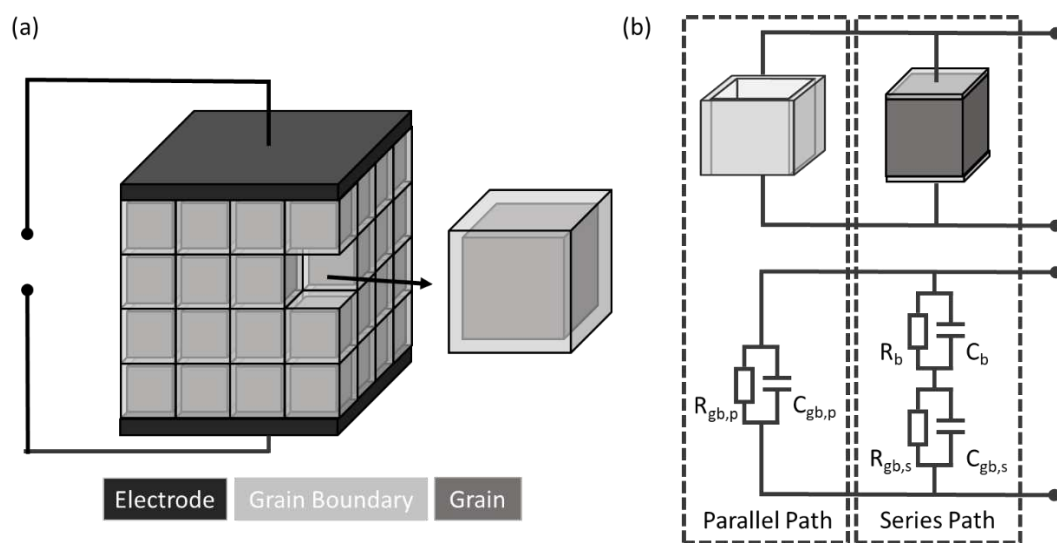


Figure 1 (a) Schematic of the Brickwork Layer Model (BLM) and (b) generic equivalent circuit associated used for data analysis.

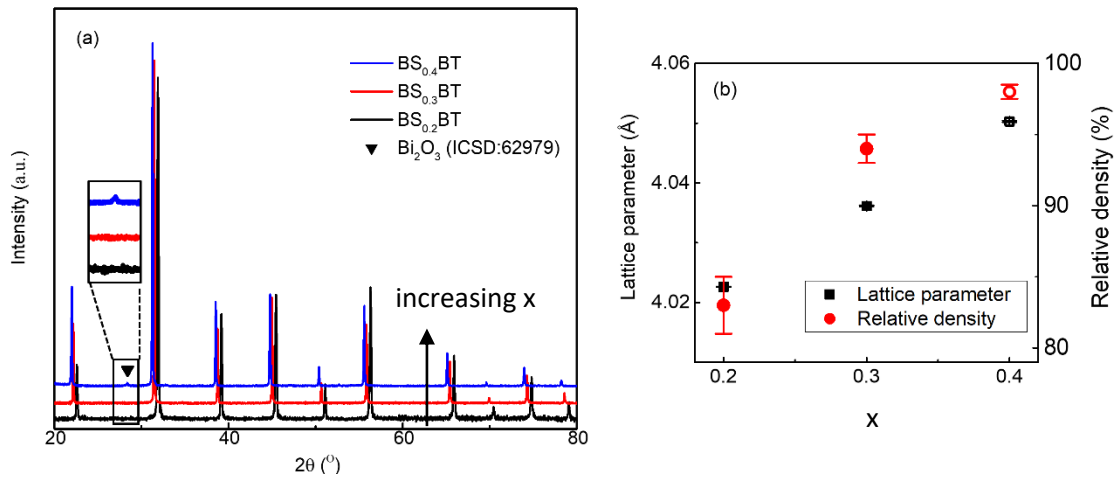


Figure 2. (a) Room temperature X-ray powder diffraction data and (b) lattice parameter and relative density for $x(BiScO_3)-(1-x)(BaTiO_3)$ (BS_xBT) crushed ceramics of $BS_{0.2}BT$, $BS_{0.3}BT$ and $BS_{0.4}BT$.

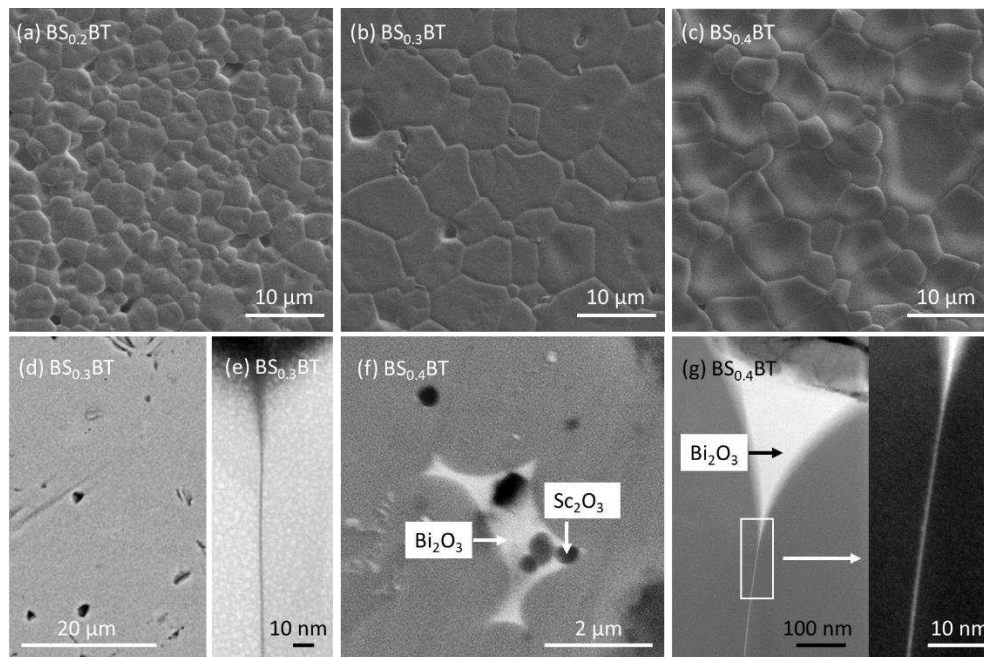


Figure 3. SEM secondary electron images of thermal etched $x(BiScO_3)-(1-x)(BaTiO_3)$ (BS_xBT) ceramics: (a) $BS_{0.2}BT$; (b) $BS_{0.3}BT$; (c) $BS_{0.4}BT$; SEM back scattered electron images of (d) $BS_{0.3}BT$ and (f) $BS_{0.4}BT$ showing the presence of Bi rich triple points in only the $BS_{0.4}BT$ sample; HAADF-STEM images of a triple pocket and grain boundary in $BS_{0.3}BT$ being deficient in atomically heavy Bi relative to the matrix and in $BS_{0.4}BT$ being rich in Bi are shown Figures (e) and (g).

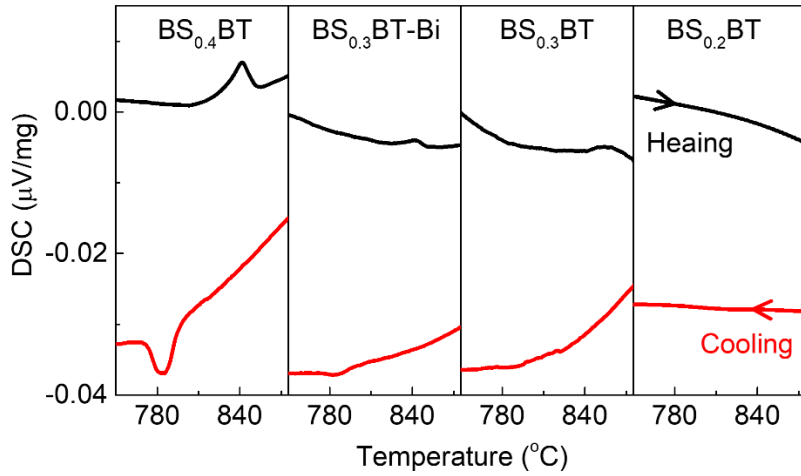


Figure 4. Differential Scanning Calorimetry results for selected $x(\text{BiScO}_3)-(1-x)(\text{BaTiO}_3)$ (BS_xBT) samples on a heating and cooling cycle in the range $\sim 750 - 880$ °C.

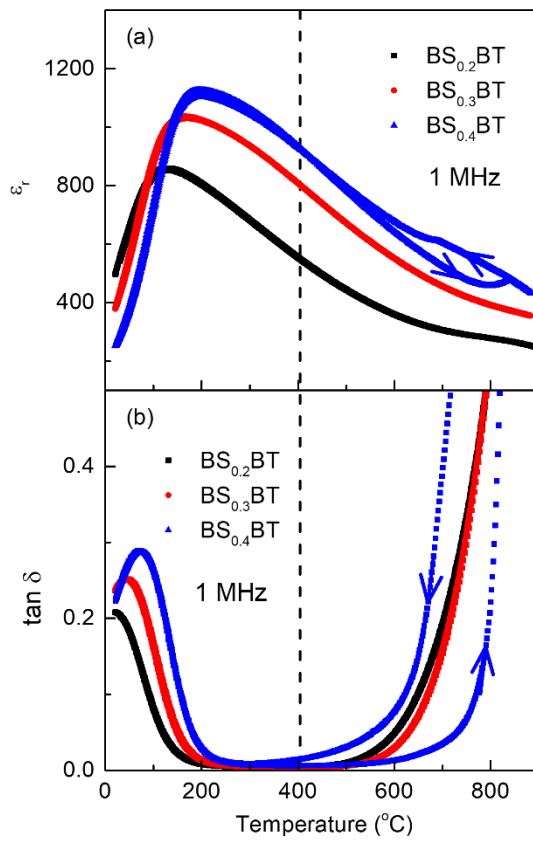


Figure 5. Temperature dependent (a) ϵ_r and (b) $\tan \delta$ (both at 1 MHz) for $x(\text{BiScO}_3)-(1-x)(\text{BaTiO}_3)$ (BS_xBT) ceramics.

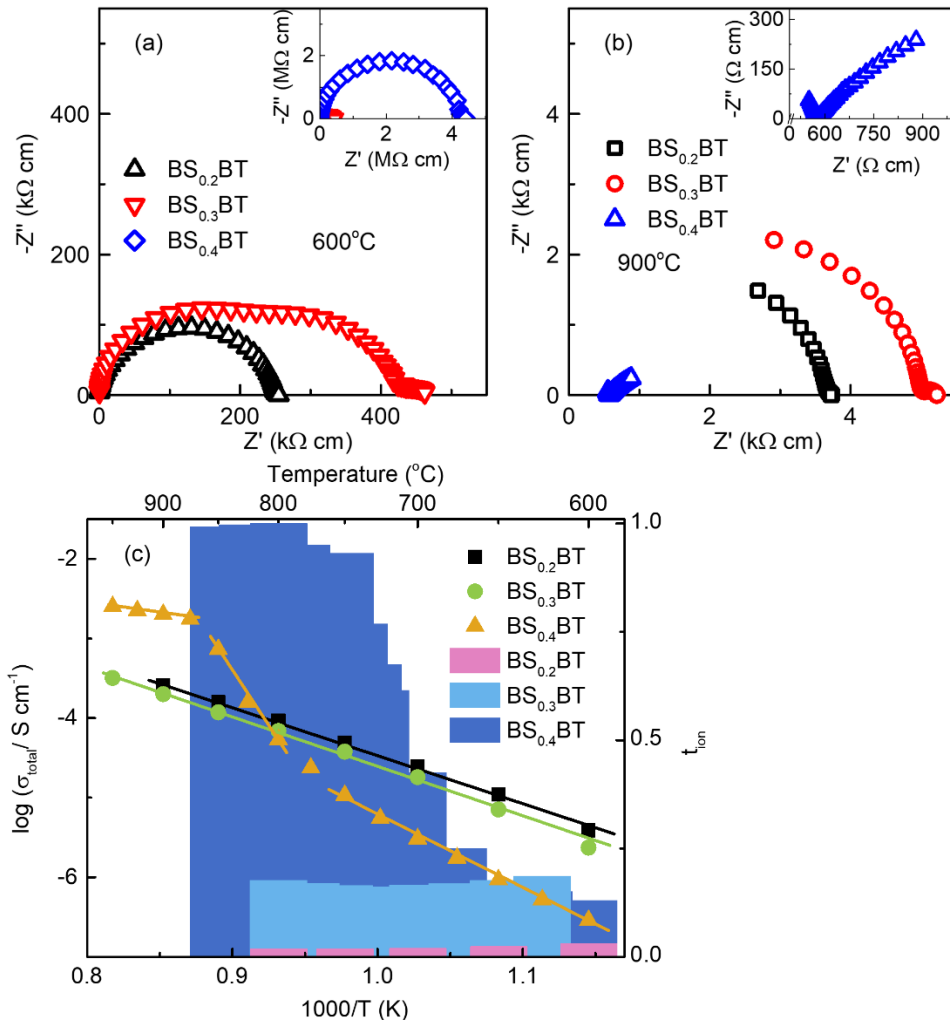


Figure 6. Z^* plot of $x(\text{BiScO}_3)-(1-x)(\text{BaTiO}_3)$ (BS_xBT) ceramics at (a) 600 °C and (b) 900 °C. (c) Arrhenius plot of total conductivity, σ_{total} , versus reciprocal temperature of BS_xBT samples.

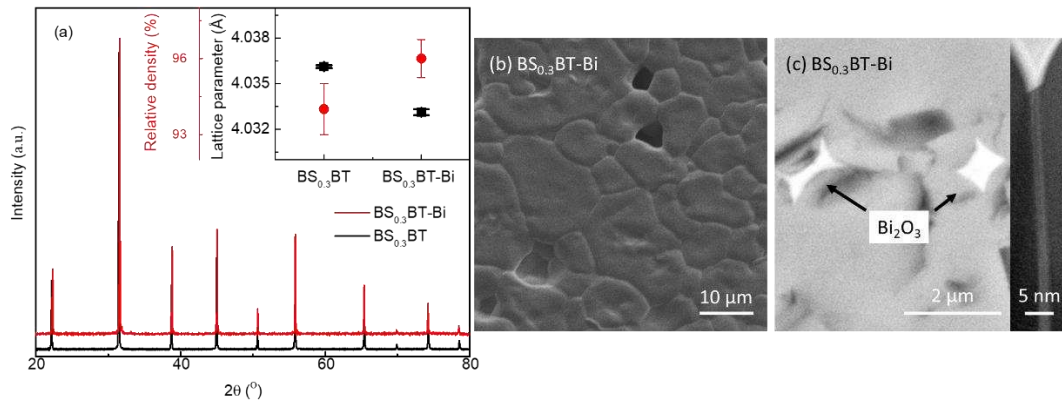


Figure 7. (a) Room temperature X-ray powder diffraction data, (b) SEM secondary electron images of thermal etched and (c) SEM back scattered electron image showing Bi-rich triple points (left) & HAADF STEM image showing Bi-rich grain boundaries (right) of $\text{BS}_{0.3}\text{BT-Bi}$ ceramic, i.e. $0.3(\text{BiScO}_3)\text{-}0.7(\text{BaTiO}_3)$ with 3wt% excess Bi_2O_3 in the starting formulation.

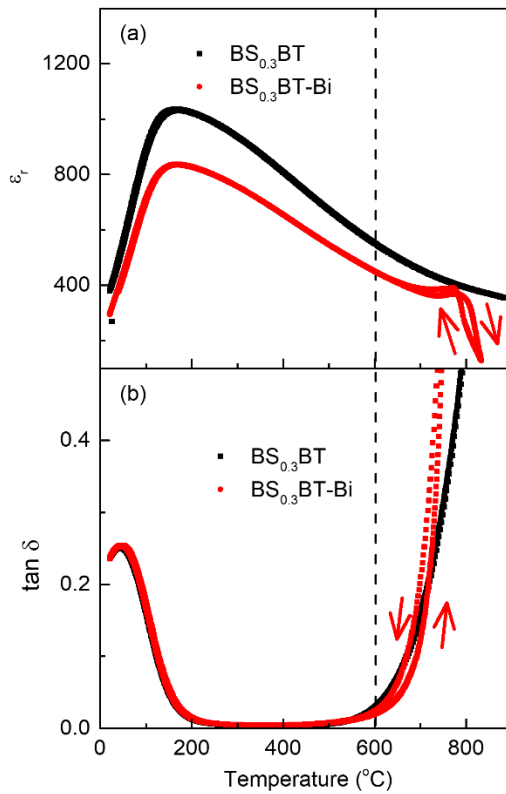


Figure 8. Temperature dependent (a) ϵ_r and (b) $\tan \delta$ (both at 1 MHz) for $\text{BS}_{0.3}\text{BT}$ and $\text{BS}_{0.3}\text{BT-Bi}$, i.e. $0.3(\text{BiScO}_3)\text{-}0.7(\text{BaTiO}_3)$ without and with 3wt% excess Bi_2O_3 in the starting formulation.

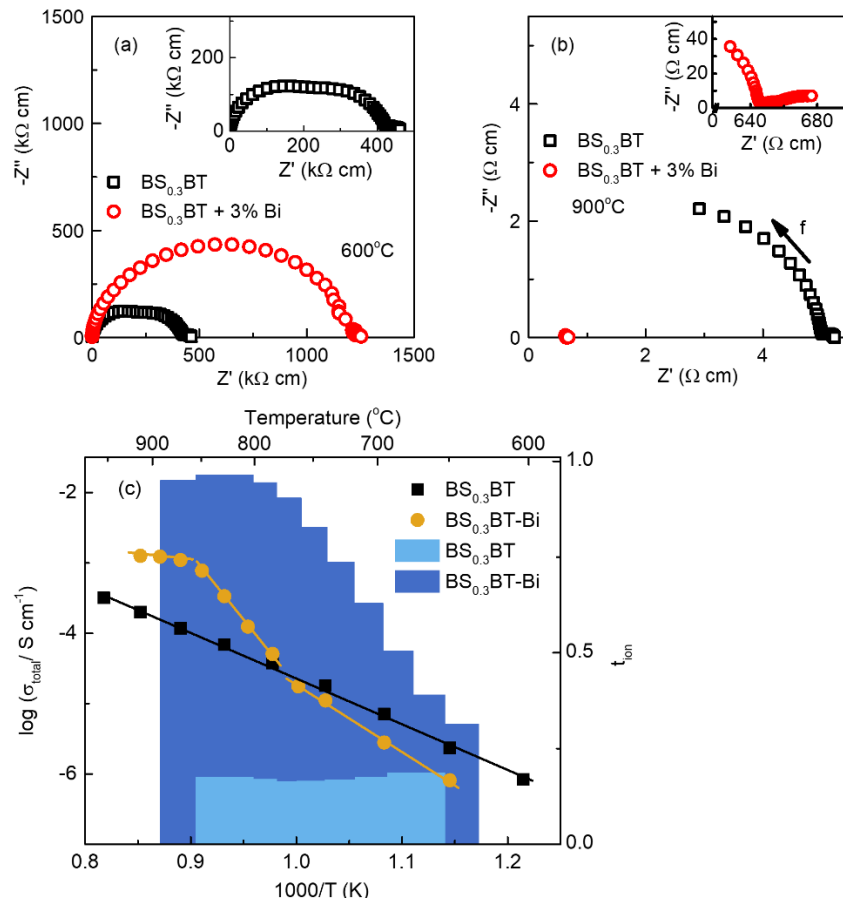


Figure 9. Z^* plot of $\text{BS}_{0.3}\text{BT}$ and $\text{BS}_{0.3}\text{BT-Bi}$ ceramics, i.e. $0.3(\text{BiScO}_3)\text{-}0.7(\text{BaTiO}_3)$ without and with 3wt% excess Bi_2O_3 in the starting formulation, at (a) 600°C and (b) 900°C . (c) Arrhenius plot of total conductivity, σ_{total} , versus reciprocal temperature for $\text{BS}_{0.3}\text{BT}$ and $\text{BS}_{0.3}\text{BT-Bi}$ ceramics.

Supplementary Figures

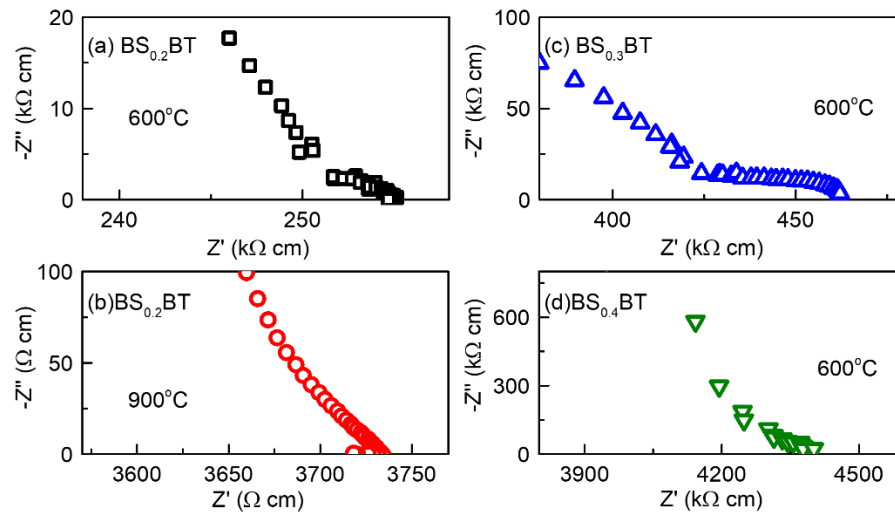


Figure S1. Expanded scale of the low frequency region in impedance Z^* plots of $x(\text{BiScO}_3)$ -(1-x)(BaTiO_3) (BS_xBT) ceramics: $\text{BS}_{0.2}\text{BT}$ ceramics at (a) 600, (d) 900 $^\circ\text{C}$ and (c) $\text{BS}_{0.3}\text{BT}$, (d) $\text{BS}_{0.4}\text{BT}$ ceramics at 600 $^\circ\text{C}$.